BJES Basrah Journal for Engineering Sciences

Basrah Journal for Engineering Sciences, Vol. 25, No. 2, (2025), 38-49

Original Article

Journal homepage: https://bjes.edu.iq/bjes
ISSN (Online): 23118385, ISSN (Print): 18146120

Simulation Absorption Refrigeration System Powered by a Solar Pond

Atyab Safaa Saleem [1]*, Salman Hashem Hammadi [2]

[1,2] *Department of Mechanical Engineering, College of Engineering, University of Basrah, Basrah, Iraq*
E-mail addresses: pgs.atyab.safaa@uobasrah.edu.iq, salman.hammadi@uobasrah.edu.iq

Article Info

Article history:
Received: 4 July 2025
Revised: 21 July 2025
Accepted: 16 August 2025
Published: 31 December 2025

Keywords:
Salt-gradient solar-pond, Transient heat and mass transfer, heat extraction, Libr-H_2O absorption refrigeration system, coefficient of performance

https://doi.org/10.33971/bjes.25.2.5

Abstract

The thermal performance of an absorption refrigeration system powered by solar pond heat was studied, simulated, and evaluated under the climatic conditions of Basra, Iraq. The simulation used MATLAB to solve the heat and mass transfer equations within the three layers of the solar pond (assuming NaCl as the salinity gradient medium) and linked them via a heat exchanger to the absorption refrigeration system to determine the temperatures supplied to the absorption cycle. The absorption cooling system operates on a lithium bromide-water pair and contains an internal heat exchanger between the generator and absorber with an assumed efficiency of 80%. The simulation was conducted over several months of the year, from March to October, and daily climatic variables such as solar radiation and ambient temperature specific to Basra were considered, allowing the system's performance to be evaluated under realistic climatic conditions. The objective was to evaluate the coefficient of performance (COP) of absorption refrigeration systems and demonstrate the feasibility of using solar ponds as a sustainable heat source for cooling in hot regions. The study demonstrated the feasibility of operating an absorption refrigeration system using the thermal energy stored in the lower layer of the solar pond, while maintaining good thermal stability in that layer throughout the day, especially in areas with high solar radiation, such as Basra. The simulation model was developed entirely in MATLAB using fundamental physical equations that describe each component of the solar pond and absorption refrigeration system, without relying on pre-existing components or tables. This provides greater modeling flexibility and a deeper understanding of system behavior under hot climate conditions.

1. Introduction

Energy consumption is an indicator of a nation's progress and advancement. Energy and its various uses constitute a fundamental pillar of civilization. The search for new and straightforward energy sources has become a pressing issue in the modern era, which suggests a potential rise in the costs of traditional energy sources. This is compounded by the possible depletion of these sources, which poses a significant threat to humanity's future. Renewable energy is essential for achieving a sustainable energy future. It offers numerous advantages over traditional energy sources. It includes diverse, abundant, and environmentally friendly technologies crucial in reducing greenhouse gas emissions. Fossil fuels are not a renewable energy source; they will quickly run out if their consumption is not rationalized. Fossil fuels have been linked to numerous environmental problems, including pollution, global warming, and the release of toxic gases into the atmosphere. Therefore, all countries must transition their economies away from fossil fuels as quickly as possible. Solar energy is distinguished from other forms because it is clean and can be harnessed without causing environmental pollution. It is freely usable but requires a specific system to harness it. Given the intermittent nature of solar energy supplies, it is essential to have a storage system that facilitates its use in a manner that meets the needs . Currently, the prices of conventional collection and storage systems are very high and sometimes uneconomical. Therefore, it is necessary to reduce their cost to make them more economically viable. It should be noted that conventional collection and storage systems account for approximately 75% of the total cost; therefore, the potential for reducing the price of a standard system does not seem particularly beneficial. Thus, a solar pond is a relatively inexpensive collection and storage system that can be used for heating, drying, cooling, solar energy generation, and other uses [1].

Arab and Middle Eastern countries, especially Iraq, have unique geographical advantages that allow them to benefit greatly from solar radiation. Iraq receives substantial solar radiation, ranging from 4908 to 66250 m W/cm ^{3}, with an average of 12 hours of sunlight daily. This is complemented by favorable climatic conditions such as low humidity, minimal cloud cover, and clear skies. These factors contribute to the high intensity of solar radiation reaching the Earth. During Iraq's hot and dry summers, the demand for cooling and air conditioning units increases during the daytime, with noon being the peak period for solar radiation. Electricity consumption rises due to the high demand for these units, with about 60% of electricity used for air conditioning, making it the largest electricity consumer in residential, commercial, and industrial sectors. Since electricity mainly relies on fossil fuels, this issue is especially severe in high-temperature regions like the Arab and Middle Eastern countries, where residents endure scorching heat for months.

To address this, harnessing solar energy for cooling offers a solution by providing heat to power absorption refrigeration systems that operate without electricity, using sources such as solar ponds. Solar energy can be broadly used, and recent

© 2025 the Authors. Published by the University of Basrah. This is an open-access article distributed under the Creative Commons Attribution License 4.0, which permits unrestricted use, distribution, and reproduction in any medium provided the original work is properly cited.

increases in air conditioning and refrigeration needs have led to higher electricity consumption. To optimize this, it's important to find alternatives to traditional vapor compression systems, which consume large amounts of electricity and damage the ozone layer. The trend now favors absorption refrigeration systems, which rely on renewable, low-cost heat sources like solar energy, making them especially suitable for countries with high solar radiation, such as Iraq. These systems are among the oldest and most widely used in refrigeration and air conditioning. They are environmentally friendly because they do not harm the ozone layer or use chlorofluorocarbons, and they are quieter than vapor compression systems.

The system consists of a thermal integration between two main components: the solar pond and the absorption refrigeration system (Libr-H_2O). The thermal energy absorbed from solar radiation is stored in the lower layer (the non-convective zone) of the solar pond, and the stored heat is then extracted from this layer via a heat exchanger installed within it.

Prasad [2] conducted a mathematical simulation to study the behavior of the solar pond and the direction of heat transfer within it, based on the assumptions. Concluded that the surface layer temperature is approximately 35°C, while the lower layer maintains a high temperature of approximately 53°C. The results showed that the thermal efficiency of the solar pond is approximately 24%.

Monjezi and Campbell [3] conducted a numerical simulation of a solar pond with a surface area of 100 square meters. The results showed that the bottom layer temperature required approximately 65 days of operation to reach its maximum value. This assumption is consistent with the experimental results of previous studies. The top layer of the pond consumes approximately 47 liters of fresh water per day. As the temperature of the bottom layer increases, its resistance to heat loss rises compared to the layers above it.

Sayer [4] company built a small-scale solar pond in Nasiriyah Governorate, Iraq, to study its performance experimentally and theoretically for 71 days. A mathematical model was developed to solve the heat transfer equations within the solar pond. To reduce the intense evaporation phenomenon on the surface of the open pond, a thin 0.5 cm paraffin layer was installed on the upper surface of the pond. The results showed that the water temperature inside the pond stabilized after approximately 50 days of operation. The water temperature in its lower layer (LCZ) could reach 90°C or higher during the summer and exceed 50°C in the winter.

Mohamed et al. [5] constructed a salinity-gradient solar pond with a surface area of 0.48 square meters and a depth of 1.1 meters. The purpose was to test the performance of the solar pond under both operating conditions, with and without heat extraction. The results showed that heat extraction from the pond improved its performance and efficiency. The solar pond's heat storage capacity increased by approximately 40% when heat extraction was performed, compared to when heat extraction was not performed. Furthermore, the overall efficiency of the solar pond increased by 29% when heat extraction was performed.

Li et al. [6] studied the performance of a 23 kW solar-powered single-effect absorption chiller system using a LiBr-H_2O working fluid. The heating mode was also investigated, analyzed, and discussed. The results showed that the maximum instantaneous cooling efficiency of the chiller (coefficient of cooling) could reach 0.6 in most conditions, while on clear, sunny days, the daily solar heat content ranged between 0.33 and 0.41. Field collector efficiencies were observed to range between 0.35 and 0.45, while chiller efficiencies ranged between 0.25 and 0.7, and daily cooling performance coefficients ranged between 0.11 and 0.27, respectively.

Yadav et al. [7] designed and fabricated a solar-powered vapor-absorption refrigeration system using lithium bromide and water as a refrigerant. The system's performance was evaluated under various operating conditions, including solar radiation and temperatures of the collector, generator, condenser, and evaporator. The system's coefficient of performance was 0.1, while its cooling capacity was 0.01 refrigeration tons. As a preliminary development, this system stands out for its unique fundamental engineering understanding. Its design also enables it to be operated using a variety of heat sources, such as solar or biomass, without the need for major design modifications, making it suitable for multiple applications such as air conditioning, refrigeration, and the refrigeration industry.

Saleh [8] conducted a study on a proposed system combining a solar pond with an absorption chiller system, aiming to investigate the potential benefits of this integration. The upper layer of the pond was used to cool the chiller, maintaining efficient performance and eliminating the need for expensive conventional cooling systems. Influencing factors, such as ambient temperature and solar radiation, were analyzed, along with pond characteristics, to optimize the performance of the proposed system, which also considered cooling and freezing temperatures. The model results showed good agreement with experimental data. A suitable site for the system was selected, such as the Dead Sea area. It was found that a 3,000 m² solar pond could provide a heat rate of 80°C, powering an absorption chiller with a cooling capacity of 126.3 kW, achieving an overall coefficient of performance of 0.183. The study demonstrated that these systems are suitable for cooling production, especially in hot regions.

This study aims to simulate and evaluate the thermal performance of an absorption refrigeration system powered by solar pond heat energy under the climatic conditions of Basra, Iraq [9]. The simulation was conducted using MATLAB to solve the heat and mass transfer equations within the three layers of the solar pond (assuming sodium chloride as the salinity gradient medium) and link them to the absorption cooling system to determine the temperatures supplied to the absorption cycle. The absorption cooling system operates on a lithium bromide-water pair and contains an internal heat exchanger between the generator and the absorber with an assumed efficiency of 80%.

The study also aims to evaluate the coefficient of performance (COP) of the absorption cooling system and demonstrate the feasibility of using solar ponds as a sustainable heat source for cooling applications in hot regions. This study addresses some research gaps represented by the scarcity of integrated numerical models that directly link the performance of solar ponds to absorption cooling systems, especially under hot climatic conditions. It also contributes to providing a dynamic simulation model that links the temperature change in the pond layers to the system performance, thus achieving a more accurate understanding of the potential for integration between the solar source and the absorption system.

2. Theoretical model

The section explains the mathematical equations for calculating heat losses (by convection, radiation, and evaporation) and the stored energy in the solar pond. Furthermore, the mathematical equations that determine the thermal efficiency of the solar pond and the temperature distribution throughout its layers are presented. The finite difference method is used to solve the obtained equations numerically. The heat extracted from the solar pond by the heat exchanger and its efficiency are calculated. A theoretical analysis of the important parameters in the absorption refrigeration system operated by the solar pond is conducted. The energy balance derived from the first and second laws of thermodynamics is carried out for each part of the absorption refrigeration system. The concentrations of lithium bromide used in the cycle are calculated, and the enthalpies and pressures are also determined.

Accurate measurement of solar radiation intensity is crucial when designing and implementing solar energy projects. Before initiating the project, the researcher aims to gather precise information about the radiation levels and their value in the work area to achieve a successful project design and ensure optimal performance during its operational phase [1]. As solar radiation penetrates the layers of the solar pond, its intensity significantly decreases with depth as the fluid layers absorb the energy. The amount of solar radiation entering the solar pond at any depth is calculated using Equation (1) [10] :

$$H_x = H_0\left(0.36 - 0.08\ \ln\left(\frac{x}{\cos\theta_r}\right)\right) \quad (1)$$

2.1. Heat transfer model

The efficiency of the solar pond is determined by the amount of solar energy entering it and the amount of heat exiting it through the upper and lower layers. Solar energy is obtained from the solar radiation incident on the pond's surface. This energy is then converted into useful energy used in various thermal applications, such as operating the absorption refrigeration system. In Figure 1, a mathematical model illustrates the behavior of heat transfer within the three layers of the solar pond. The solar radiation H_0 cells on the surface of the solar pond and heat the water molecules in the upper layer of the solar pond (UCZ). Then, the transfer of thermal energy from the upper layer to the middle layer begins with the movement of hot water molecules from the upper layer to the middle layer (NCZ). Similarly, thermal energy is transferred to the lower layer of the solar pond (LCZ). It should be noted that thermal conduction transfers heat within the layers of the solar pond.

2.1.1. Energy balance for UCZ:

The energy entering a solar pond's surface equals the sum of the energy leaving the pond and stored in it, as in Equation (2):

$$\textit{Energy in} = \textit{Energy out} + \textit{Energy stored} \quad (1)$$

$$\left[H_0 + q_{cond1}\right] = \left[H_1 + q_{loss}\right] + \rho\ C_P\ \frac{\partial T}{\partial t} X_{UCZ} \quad (3)$$

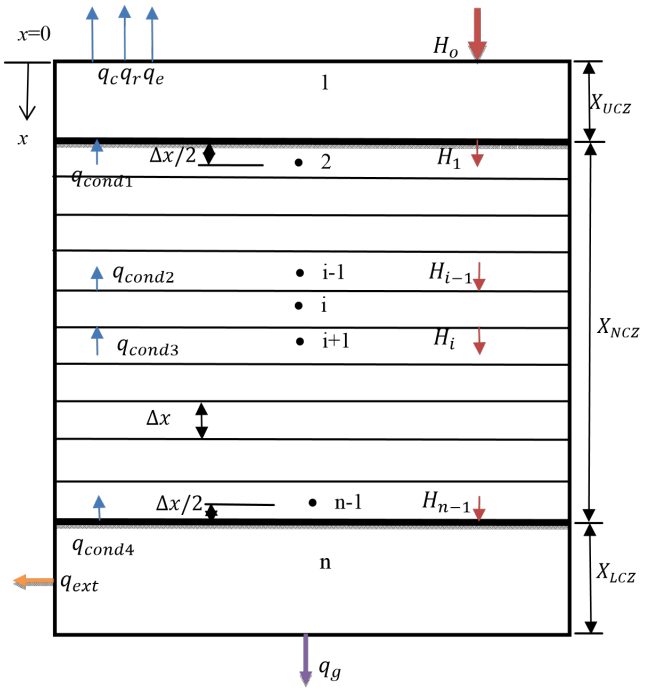

Fig. 1 Mathematical model of solar pond, X_{UCZ} = 0.1 m, X_{NCZ} = 0.6 m, X_{LCZ} = 0.3 m.

Where:

$$q_{cond1} = \frac{k\left(T_2^j - T_1^j\right)}{\frac{\Delta x}{2}} \quad (4)$$

$$q_{loss} = q_c + q_r + q_e \quad (5)$$

Where q_{loss} represent the total heat loss from the surface of the solar pond results from convection, radiation, and evaporation, respectively. The heat transfer by convection from the upper layer to the atmosphere depends on the wind speed and the temperature change between the atmosphere and the water surface in the solar pond, as in Equation (6):

$$q_c = h(T_1 - T_a) \quad (2)$$

The convection heat transfer coefficient can be determined by Equation (7) [10] :

$$h = 5.7 + 3.8\ V \quad (3)$$

The Equation (8) is used to calculate the radiation heat loss:

$$q_r = \sigma\ \varepsilon_w \left\{(T_1 + 273)^4 - \left(T_{sky} + 273\right)^4\right\} \quad (4)$$

Where the σ represents the Stefan-Boltzmann constant, equal to $5.67 \times 10^{-8} W.m.K^{-4}$ and ϵ_w the emissivity of water is equal to 0.83 and T_{sky} refer to the sky temperature calculated by Equation (9) [11]:

$$T_{sky} = T_a - \left(0.55 + 0.061\sqrt{P_a}\right)^{0.25} \quad (5)$$

Where T_a and T_{sky} in °C and P_a in mmHg.

The Equation (10) calculates the heat loss by the evaporation phenomenon of water [10] as :

$$q_e = \frac{L_v\, h\, (P_1 - P_a)}{1.6\, C_s P_{atm}} \quad (6)$$

Where:

$$P_1 = exp\left(18.403 - \frac{3885}{T_1 + 230}\right) \quad (7)$$

$$P_a = RH * exp\left(18.403 - \frac{3885}{T_a + 230}\right) \quad (8)$$

The finite difference Equation for the upper convective-zone layer temperature can be obtained from (3) [12] :

$$T_1^{j+1} = T_1^j + \frac{\Delta t}{\rho C_P X_{UCZ}}\left[(H_0 - H_1) + k\left(\frac{T_2^j - T_1^j}{\frac{\Delta x}{2}}\right) - q_{loss}^j\right] \quad (9)$$

2.1.2. Energy balance for NCZ:

The Non-convective zone has been divided into multiple layers (2 to n-1), where the energy balance for the non-convective zone layers can be written as Equation (14):

$$[H_{i-1} + q_{cond3}] = [H_i - q_{cond2}] + \rho C_P \frac{\partial T}{\partial t}\Delta x \quad (10)$$

2.1.3. Energy balance for LCZ:

The energy balance for the LCZ layer of the solar pond can be written as Equation (15):

$$[H_{n-1}] = \left[q_{cond4} + q_g\right] + \rho C_P \frac{\partial T}{\partial t} X_{LCZ} \quad (11)$$

The heat loss by conduction from the lower convective zone to the non-convective zone at the interface is calculated as Equation (16):

$$q_{cond4} = -k \frac{\partial T_n^j}{\partial x}|_{x=X_{UCZ}+X_{NCZ}} \quad (12)$$

The heat loss to the ground can be calculated as:

$$q_g = -k_g \frac{\partial T_n^j}{\partial x}|_{x=X_{UCZ}+X_{NCZ}+X_{LCZ}} \quad (13)$$

By substituting (16) and (17) in (15) and simplifying, the finite difference for the lower convective zone temperature is given as [12]:

$$T_n^{j+1} = T_n^j + \frac{\Delta t}{\rho C_P X_{LCZ}}\left[(H_{n-1}) - k\left(\frac{T_n^j - T_{n-1}^j}{\frac{\Delta x}{2}}\right) - U_g\left(T_n^j - T_g^j\right)\right] \quad (14)$$

Where U_g the ground's overall heat transfer coefficient can be calculated by Equation (19) [13]:

$$U_g = \frac{k_g}{L_g} \quad (15)$$

2.2. Mass transfer model

During the operation of the solar pond, many physical processes occur. Mass transfer by convection occurs in the UCZ and LCZ, and mass transfer by diffusion occurs in the NCZ. A density gradient can be developed by molecular diffusion. In the selected model, the system's total mass in the controlling volume is constant, and the mass transfer process occurs due to molecular diffusion. Mass transfer processes happen in a direction independent of thermal processes. According to these assumptions, one-dimensional mass diffusion in the direction of the x-axis for the differential volume element of the thickness, Δx, is written as:

$$\frac{\partial}{\partial x}\left(D \frac{\partial C(x,t)}{\partial x}\right) = \frac{\partial C(x,t)}{\partial t} \quad (16)$$

Where the C is the salt concentration in kg/m³, the diffusion coefficient of salt (D) is $3*10^{-9}$ m²/s, according to Equation (21) [14]:

$$C_i^{j+1} = C_i^j + \frac{D\,\Delta t}{\Delta x^2}\left[C_{i-1}^j - 2 * C_i^j + C_{i+1}^j\right] \quad (17)$$

This Equation represents the salt concentration in NCZ [12]. Initial conditions can be imposed to be $10\ kg/m^2$ at the upper convective zone and $200\ kg/m^2$ at the lower convective zone.

The boundary conditions for the mass transfer Equation are:

(a) In the upper layer of the solar pond, the mass balance is given by:

$$D \frac{\partial C}{\partial x} = \frac{\partial C}{\partial t} X_{UCZ} \quad (18)$$

(b) In the lower layer of the solar pond, the mass balance is given by:

$$-D \frac{\partial C}{\partial x} = \frac{\partial C}{\partial t} X_{LCZ} \quad (19)$$

2.3. Extraction and consumption of heat from a solar pond

The heat extraction rate from a solar pond is calculated by [15]:

$$Q = A_o U \times LMTD \quad (20)$$

Where A_oU and LMTD equal to:

$$A_oU = \frac{1}{R_{overall}} \quad (21)$$

$$LMTD = \frac{[T_o - T_i]}{\ln\left[(T_P - T_i)/(T_P - T_o)\right]} \quad (22)$$

The energy extracted from the pond and consumed in the external heat exchanger and piping system outside the solar pond is obtained from the following Equation [16]:

$$Q = \dot{m} C_P (T_o - T_i) \quad (23)$$

The Pond Efficiency can be calculated from the following Equation [15]:

$$\eta = \frac{\dot{m} C_P (T_o - T_i)}{H_{Avg} \times A_{sp}} \quad (24)$$

The monthly solar radiation rate H_{Avg} is calculated from the Equation (29), which is solved using the trapezoidal method:

$$H_{Avg} = \frac{1}{t_s - t_r} \int_{tr}^{ts} H_0 dt \quad (25)$$

The overall heat transfer coefficient can be calculated from:

$$R_{overall} = R_P + R_{fo} + R_{tube} + R_{fi} + R_{water} \quad (26)$$

$$R_{overall} = \frac{1}{h_o A_o} + \frac{R_{fo}}{A_o} + \frac{1}{2\pi K_c L} \ln\left(\frac{d_o}{d_i}\right) + \frac{R_{fi}}{A_i} + \frac{1}{h_i A_i} \quad (27)$$

Figure 2 represents an absorption refrigeration system powered by a solar pond, where the heat exchanger extracts heat from the solar pond and transfers it to the generator to power the absorption cycle.

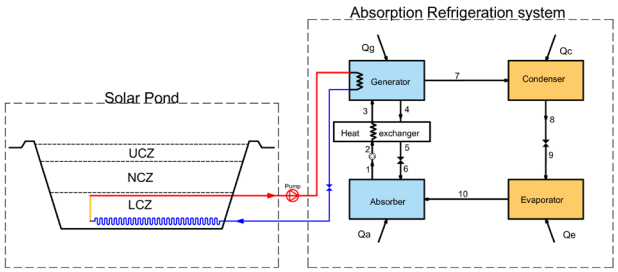

Fig. 2 Absorption Refrigeration System Powered by a Solar Pond.

2.4. Heat balance of absorption refrigeration system

Figure 3 shows the absorption refrigeration cycle, in which the working fluid flows within a closed system and interacts with the environment, causing heat and work transfer. The high-pressure refrigerant (water) (8) passes from the condenser to the evaporator through the expansion valve (9), which reduces the refrigerant pressure to a low pressure to enter the low-pressure evaporator. The refrigerant evaporates in the evaporator as a result of absorbing heat Q_E.

The medium is cooled, resulting in low-pressure vapor (10) passing to the absorber. The absorption process occurs by reacting with the absorbent material, lithium bromide salt, which produces heat Q_A . and turns into a weak solution of (Libr-H_2O). The weak solution (Libr.H_20) exits from the absorber (1) to the pump, where its pressure increases, and then enters the heat exchanger (2) to raise its temperature, and then enters the generator (3). The weak solution is heated in the generator by the high-temperature initiators Q_G comes from the solar pond, so the solution decomposes. The absorbent material (LiBr salt) leaves the generator (4) at a high concentration (pure LiBr salt), enters the heat exchanger, and exits from it (5) at a lower temperature, then goes to the expansion valve to decrease its pressure.

The strong solution flows and returns to the absorber (6). As for the coolant (water), it evaporates as pressure rises and it heads to the condenser (7) where it condenses and turns into a liquid at high pressure, resulting in the release of heat Q_C. Thus, the cycle is completed and repeated in the same stages. According to the ASHRAE definition, a heat exchanger can be added to improve the system's performance.

The heat released to the environment equals the heat transferred from the absorber and the condenser under stable conditions. The total energy balance equation for the entire cycle, according to the first law, is given as Equation (32):

$$\dot{Q}_C + \dot{Q}_A = \dot{Q}_G + \dot{Q}_E + \dot{W}_P \quad (28)$$

Neglecting the work of the solution pump due to its small size compared to the system's inputs and outputs, the absorption cycle performance coefficient is calculated based on the heat extracted from the evaporator and the heat input to the generator. The COP is given by Equation (33):

$$COP = \frac{\dot{Q}_E}{\dot{Q}_G} \quad (29)$$

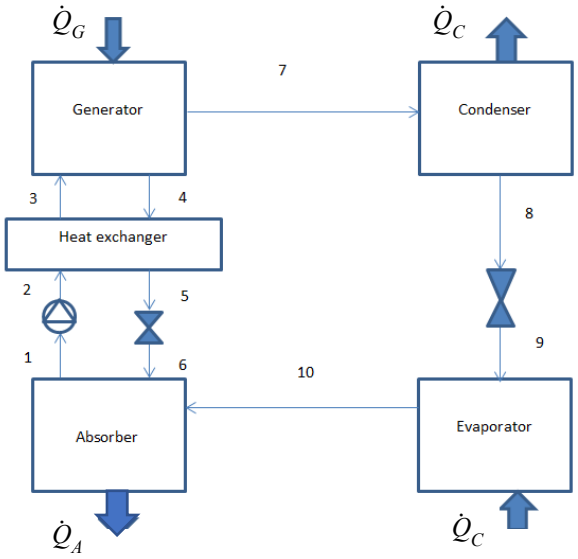

Fig. 3 Absorption Refrigeration System.

2.5. The mass and energy balance equations

Mass and energy balances must be carried out in each component to conduct a system analysis [24].

Mass and energy balances in the absorber, Figure 4 shows the inputs and outputs of the absorber.

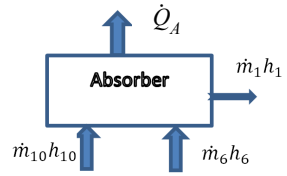

Fig. 4 Input and output of the absorber.

Equation (34) shows the mass balance where the mass flow rate entering the absorber equals the mass flow rate leaving it.

$$\dot{m}_1 = \dot{m}_{10} + \dot{m}_6 \quad (30)$$

From the heat balance of the energy entering and exiting the absorber, the amount of heat removed from the absorber can be calculated using Equation (35):

$$\dot{Q}_A = \dot{m}_{10} h_{10} + \dot{m}_6 h_6 - \dot{m}_1 h_1 \quad (31)$$

2.5.1. Mass and energy balances in the pump

Equation (36) shows that the mass flow rate entering the pump equals the mass flow rate exiting it.

$$\dot{m}_1 = \dot{m}_2 \quad (32)$$

The work output from the pump is calculated by Equation (37).

$$\dot{W}_P = \dot{m}_1 (h_2 - h_1) \quad (33)$$

2.5.2. Mass and energy balances in the heat exchanger:

Figure 5 shows the inputs and outputs of the heat exchanger.

Fig. 5 Input and output of the heat exchanger.

Whereas the mass flow rate leaving the heat exchanger equals the mass flow rate entering it. As in Equation (38):

$$\dot{m}_2 = \dot{m}_3 , \dot{m}_4 = \dot{m}_5 \quad (34)$$

The energy entering the heat exchanger is equal to the energy leaving it, as in Equation (39):

$$\dot{m}_2(h_2 - h_3) = \dot{m}_4(h_4 - h_5) \quad (35)$$

Rearranging (39) to get Equation (40) as:

$$h_3 = h_2 - \frac{\dot{m}_4}{\dot{m}_2}(h_4 - h_5) = h_2 - \frac{\dot{m}_{ss}}{\dot{m}_{ws}}(h_4 - h_5) \quad (36)$$

2.5.3. Mass and energy balances in the generator

Figure 6 represents the generator inputs and outputs.

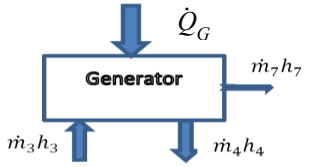

Fig. 6 Input and output of the generator

In Equation (41), $\dot{m}_3$ represents the mass flow rate entering the generator, while the sum of $\dot{m}_4$ and $\dot{m}_7$ represents the mass flow rate exiting the generator.

$$\dot{m}_3 = \dot{m}_4 + \dot{m}_7 \quad (37)$$

To calculate the mass balance of a lithium bromide-water solution, we multiply the mass flow rate by the solution concentration, as in Equation (42):

$$\dot{m}_3 x_3 = \dot{m}_4 x_4 + \dot{m}_7 x_7 \quad (38)$$

To calculate the rate of thermal energy entering the generator, we use Equation (43):

$$\dot{Q}_G = \dot{m}_4 h_4 + \dot{m}_7 h_7 - \dot{m}_3 h_3 \quad (39)$$

From Equations (41) and (42), the mass flow rate of the strong solution and the weak solution can be obtained from Equations (44) and (45):

$$\dot{m}_3 = \dot{m}_{ss} = \dot{m}_{ref.}\frac{x_4 - x_7}{x_4 - x_3} \quad (40)$$

$$\dot{m}_4 = \dot{m}_{ws} = \dot{m}_{ref.}\frac{x_3 - x_7}{x_4 - x_3} \quad (41)$$

Since state 7 is pure water (i.e., $x_7 = 0$) The above equations can be written as in Equation (46):

$$\dot{m}_3 = \dot{m}_{ss} = \dot{m}_{ref.}\frac{x_4}{x_4 - x_3} , \dot{m}_4 = \dot{m}_{ws} = \dot{m}_{ref.}\frac{x_3}{x_4 - x_3} \quad (42)$$

The solution concentration x is defined from Equation (47):

$$x = \frac{mass\ of\ refrigerant}{mass\ of\ solution\ (refrigerant + absorbent)} \quad (47)$$

The strong and weak solution concentrations are given by Equations (48) and (49) [17]:

$$X_{ws} = 49.04 + 1.125T_A - T_E/134.65 + 0.47T_A \quad (43)$$

$$X_{ss} = \frac{49.04 + 1.125T_G - T_C}{134.65 + 0.47T_G} \quad (44)$$

2.5.4. Mass and energy balances in the condenser:

Figure 7 represents the condenser inputs and outputs.

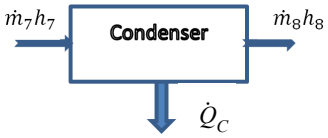

Fig. 7 Input and output of the condenser.

Equation (50) shows that the mass flow rate remains constant at the condenser's entrance and exit and represents the refrigerant's mass flow rate.

$$\dot{m}_7 = \dot{m}_8 = \dot{m_{ref.}} \quad (45)$$

The amount of heat released from the condenser is calculated using Equation (51):

$$\dot{Q}_C = \dot{m}_{ref.}(h_7 - h_8) \quad (46$$

2.5.5. Mass and energy balances in the expansion valves:

Figure 8 represents the inputs and outputs of the expansion valve.

Fig. 8 Input and output of the expansion valves.

The mass flow rate remains unchanged when entering the expansion valve, staying constant as shown in Equation (52):

$$\dot{m}_8 = \dot{m}_9 = \dot{m_{ref.}} , \dot{m}_5 = \dot{m}_6 = \dot{m}_{ws} \quad (47)$$

The enthalpy also remains constant, as in equation (53):

$$h_8 = h_9 , \ h_5 = h_6 \quad (48)$$

2.5.5. Mass and energy balances in the evaporator

The Fig. 9 shows the inputs and outputs of the evaporator.

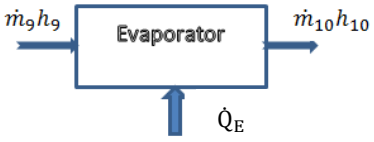

Fig. 9 Input and output of the evaporator.

The mass flow rate is not affected when entering the evaporator and is equal to the mass flow rate of the refrigerant, as in Equation (54).

$$\dot{m}_9 = \dot{m}_{10} = \dot{m}_{ref.} \quad (49)$$

The amount of heat absorbed by the refrigerant in the evaporator is calculated from Equation (55):

$$\dot{Q}_E = \dot{m}_{ref.}(h_{10} - h_9) \quad (50)$$

To calculate the saturation vapor pressure at the condenser and evaporator, use the Equation (56) [18]:

$$P_s = 610.94e^{\frac{17.625T}{T+273.86}} \quad (51)$$

To calculate the enthalpy of an aqueous lithium bromide solution, use the Equation (57) [19]:

$$h = \sum_0^4 A_n X^n + T\sum_0^4 B_n X^n + T^2 \sum_0^4 C_n X^n \quad (52)$$

A_n, B_n, C_n are constants that can be obtained from Table 1.

Table 1. Merkel diagram, only use when 15<T<165℃ and 45<X<70% of LiBr

A_n	value	B_n	value	C_n	value
A_0	-2024.33	B_0	18.2829	C_0	-0.037008214
A_1	163.309	B_1	-1.1691757	C_1	0.0028877666
A_2	-4.88161	B_2	0.03248041	C_2	-8.1313015E-5
A_3	0.06302948	B_3	-4.034184E-4	C_3	9.9116628E-7
A_4	-2.913705E-4	B_4	1.8520569E-6	C_4	-4.4441207E-9

State 7 is pure water produced in the generator. This state is often superheated, and its enthalpy is difficult to find using thermodynamic steam tables. To overcome this problem, the enthalpy of superheated steam at relatively low pressure can be found using Equation (58):

$$h = 2501.3 + 1.86T \quad (53)$$

The following equation gives the enthalpy at the outlet of the condenser [17]:

$$h_8 = 4.1845 * T_c \quad (54)$$

The enthalpy at the outlet of the evaporator is given as follows [19]:

$$h_{10} = -0.00125397 * T_E^2 + 1.88060937 * T_E + 2500.559 \quad (55)$$

3. Results and discussion

3.1. Solar pond

3.1.1. Temperature distribution in the layers of the solar pond

Figure 10 illustrates the temporal temperature behavior of the three layers of the solar pond. The lower convective zone (LCZ) exhibits the highest temperatures, peaking at 125°C in July. This indicates effective heat storage during this month. The middle non-convective zone (NCZ) records moderate temperatures and acts as an insulating barrier, reducing heat loss from the LCZ to the UCZ. The upper convective zone (UCZ) exhibits the lowest temperatures due to its direct exposure to the outside atmosphere and the heat exchange that occurs with it. This thermal stratification of the solar pond confirms its effectiveness in achieving thermal insulation and long-term heat storage. The consistency between solar radiation and temperature behavior, particularly the delayed response in the lower LCZ, reflects the pond's ability to store heat and delay its loss. This enhances the system's reliability as a heat source for absorption refrigeration systems, particularly during periods of fluctuating solar radiation.

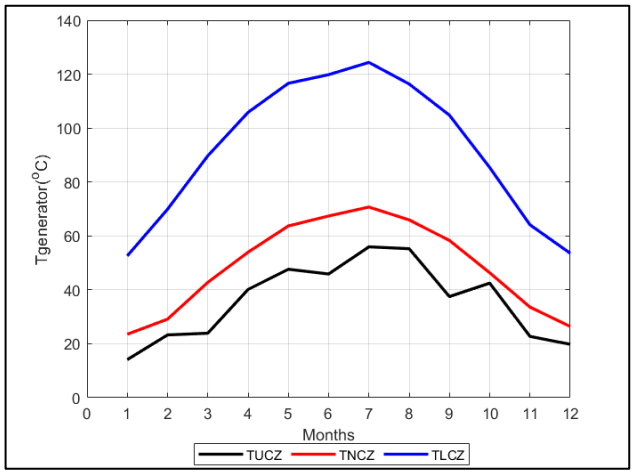

Fig. 10 Temperature distribution in the layers of the solar pond during a year.

3.1.2. Thermal distribution inside the solar pond:

Figure 11 illustrates the relationship between temperature (°C) and depth (m) of the solar pond at the end of March, May, July, and September. This distribution highlights the presence of three thermal zones within the pond, reflecting the system's thermal performance. The surface convection zone (UCZ) extends from the surface down to a depth of 0.1 meters and maintains a nearly constant temperature. The middle zone (NCZ) stretches from 0.1 to 0.7 meters and displays a distinct thermal gradient. This gradient arises from the suppression of convection due to the salinity concentration gradient, which acts as a natural thermal insulator, inhibiting heat loss from the lower layer to the external environment. The lower storage zone (LCZ) lies between 0.7 meters and the pond's bottom at a depth of 1 meter and is characterized by a relatively high and stable temperature.

March recorded the lowest temperature gradient with depth, with surface temperatures starting at 47°C and gradually increasing in the middle layer, reaching approximately 92°C at the beginning of the lower layer at a depth of 0.7 meters, then remaining constant at that depth up to 1 meter. The temperature decrease in the upper layers can be attributed to the cooler weather this month, which directly impacts heat transfer in the upper layers. In May, temperatures increase significantly compared to March, with the upper layer starting at 54°C at a depth of 0-0.1 meters. The temperature fluctuates between 54°C and 119°C in the middle layer before stabilizing at 119°C in the lower layer at a depth of 0.7-1 meters. This trend signals the onset of summer and an increase in solar radiation intensity.

July records the highest temperatures of all months, with the curve beginning at 60.5°C in the upper layer at a depth of 0-0.1 meters, gradually rising to 126°C at a depth of 0.7

meters, then stabilizing at this temperature in the lower layer between 0.7-1 meters. This reflects the peak of solar radiation, increased atmospheric temperatures, and improved thermal storage efficiency in the lower layer compared to previous months. In September, the curve is positioned midway between May and July, with temperatures beginning at 55°C in the upper layer and gradually ascending through the middle layer to stabilize at approximately 108°C in the lower layer. This lower temperature, compared to July, is due to the reduction in solar radiation at the end of summer, although the pond retains some of the heat from previous months.

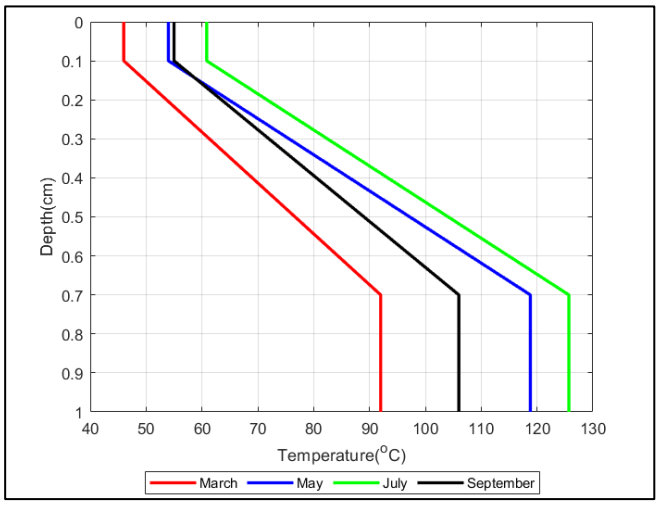

Fig. 11 Temperature distribution of the layers of the solar pond with depth at the end of March, May, July, and September.

3.1.3. Solar pond concentration

Figures 12 and 13 show the temporal variation in the salt (sodium chloride) concentration gradient in the three layers of the solar pond: the upper surface zone (UCZ), the middle non-convective zone (NCZ), and the lower convective zone (LCZ), during March and July. In both figures, the concentration in the lower convective zone (LCZ) remains nearly constant at a high value of about 200 kg/m³, indicating stable salt accumulation in the lower layer of the pond due to limited mixing and salt saturation in that layer. The middle non-convective zone (NCZ) shows a nearly constant concentration between 95-97 kg/m³ throughout the month, reflecting its unique role as a diffusion barrier that limits convective heat loss. Clear differences in the concentration behavior within the upper convective zone (UCZ) are observed between the two months.

In March (Fig. 12), the salt concentration decreases slightly in the first days, then gradually increases to about 25 kg/m³. In July (Fig. 13), salt concentration steadily rises from roughly 10 kg/m³ to 28 kg/m³. This increase results from higher evaporation rates caused by elevated temperatures, which lead to increased salt concentrations at the surface. These findings confirm the long-term stability of the salt gradient in the layers of the solar pond, especially under the climatic conditions of Basrah Governorate. The rise in the salinity of the upper layer during the hot months is considered in system operation to ensure high thermal efficiency and prevent salt deposition.

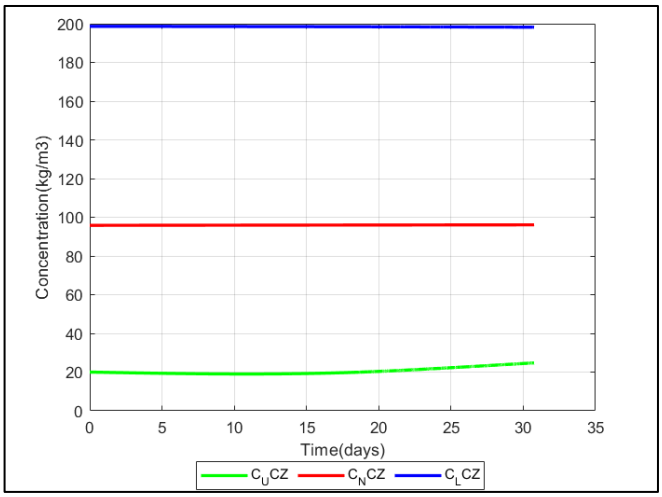

Fig. 12 Solar Pond layers concentrations in March.

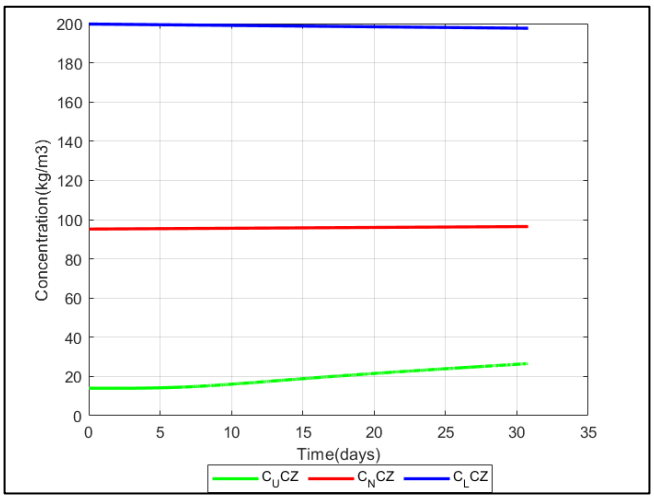

Fig. 13 Solar Pond layers concentrations in July.

3.1.4. Solar pond efficiency

In March (Fig. 14), efficiency started at zero and gradually increased, reaching approximately 0.56 by the end of March. This trend is attributed to improved solar radiation conditions and moderate temperatures. In July (Fig.15), the highest efficiency was recorded, surpassing 0.95, signifying optimal performance for the solar pond. This is attributed to the peak of summer solar radiation, where the available solar energy is maximally utilized.

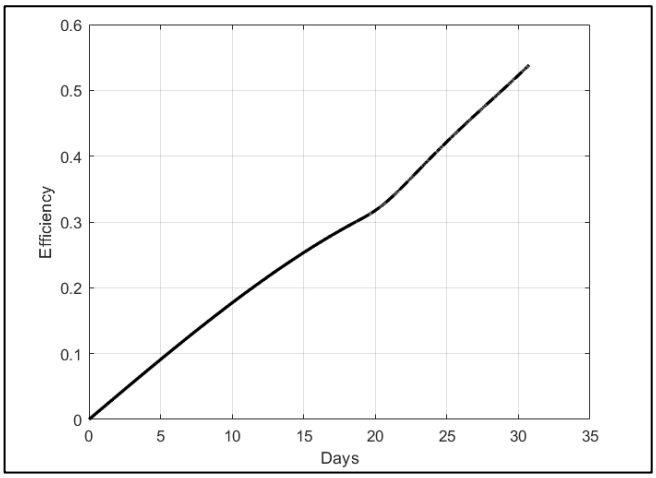

Fig. 14 Solar Pond efficiency in March.

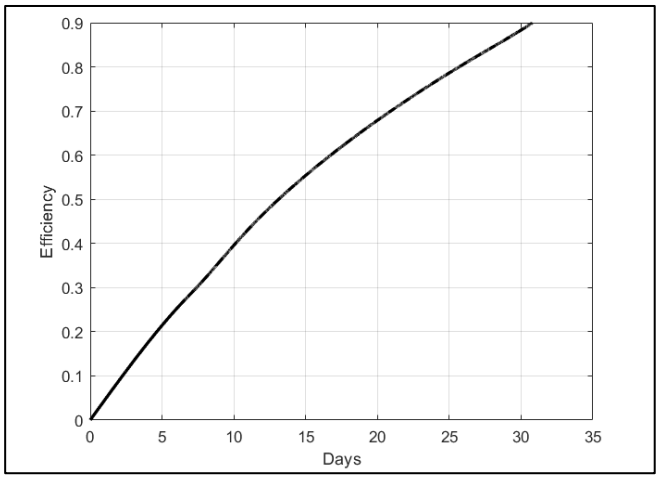

Fig. 15 Solar Pond efficiency in July.

3.1.5. Verifying the temperatures in the upper and lower layers

Figure 16 shows the experimental annual temperature distribution and simulation results for the upper (UCZ) and lower (LCZ) layers of the El Paso Solar Pond [15]. The El Paso Pond is a research and development project managed by the University of Texas at El Paso. The project began in 1983, and the pond has been operational since 1985. It covers an area of 3,000 square meters and reaches a depth of 3.25 meters. It consists of three zones: the upper zone (UCZ) with a depth of 0.7 meters, the middle zone (NCZ) at a depth of 1.2 meters, and the lower zone (LCZ) at a depth of 1.35 meters. The simulations were performed using a model based on the annual temperatures of the El Paso Pond (1991-1993) and incorporated weather data from El Paso in MATLAB. The lower layer (LCZ) exhibits relatively constant thermal behavior, with a temperature range of approximately 70 to 97°C. Good agreement was observed between the simulation and experimental results, particularly from March to August, characterized by high solar radiation rates. Slight differences were noted between the experimental and theoretical values, possibly due to changes in the properties of the pond solution or the oversight of certain weather factors in the simulation model. In the upper layer, temperatures drop significantly, ranging from 11 to 38°C. Figure 16 shows good agreement between the simulation results and the experimental data, with slight differences across different months, where the simulation's temperature values were higher than those observed in the experimental data. This discrepancy may be due to simplifications in the mathematical model or other factors related to climate change. Conclude that the MATLAB model for the solar pond effectively simulates two separate ponds of different sizes.

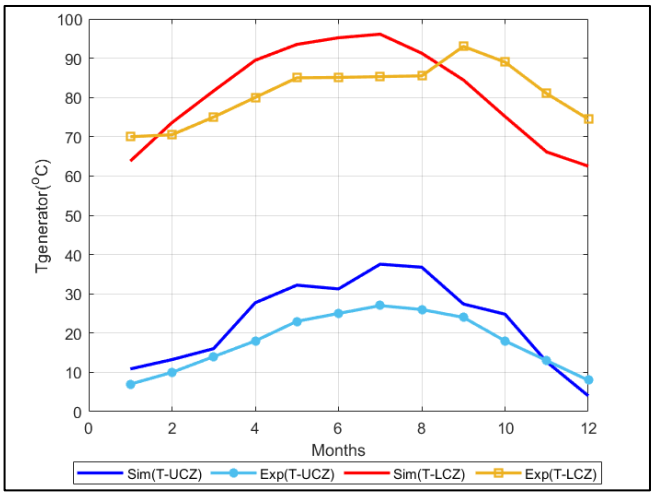

Fig. 16 Simulated and experimental annual temperature [15] of the El Paso solar pond using MATLAB.

3.2. Absorption refrigeration system

3.2.1. Input Energy to the generator

In March (Fig. 17), the results showed a gradual increase in $\dot{Q}_G$ values as the generator temperature rose from 65°C to 75°C in March. During July (Fig. 18), thermal generation peaked, with $\dot{Q}_G$ reaching a maximum value of approximately 255 watts in July. This peak is attributed to the intense solar radiation during that month, which led to an increase in thermal storage in the solar pond and improved efficiency.

3.2.2. Evaporator capacity

In March (Fig.19), the evaporator discharge load begins at a low level and gradually increases to 55 watts, with a generator temperature reaching 74.8°C by the end of the month. This direct proportion indicates a steady improvement in system performance as temperature rises, although the recorded values remain low due to limited solar energy storage in March.

July (Fig. 20) was the month with the best thermal performance, exceeding 139 watts by the end of the month. This peak was due to ideal climatic conditions, including high solar radiation and temperatures.

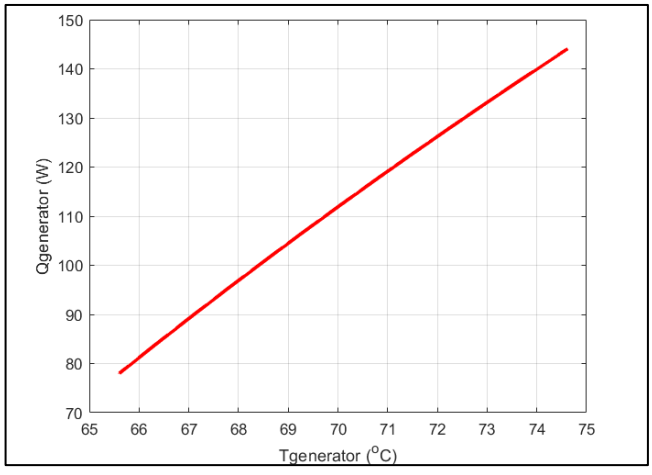

Fig. 17 The variation of $\dot{Q}_G$ with the generator temperature in March.

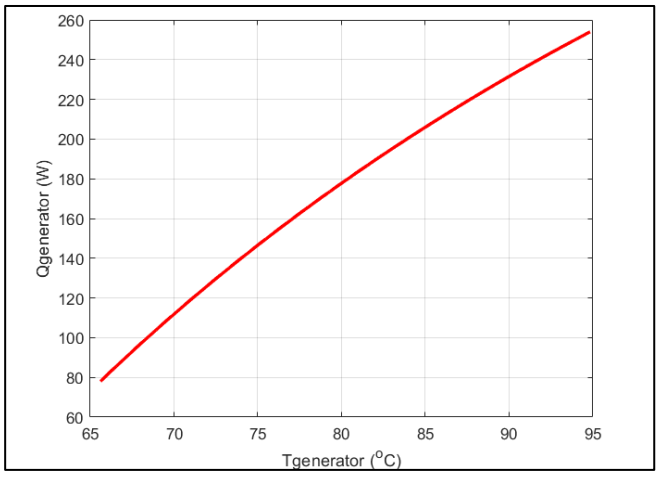

Fig. 18 The variation of Q_G with the generator temperature in July.

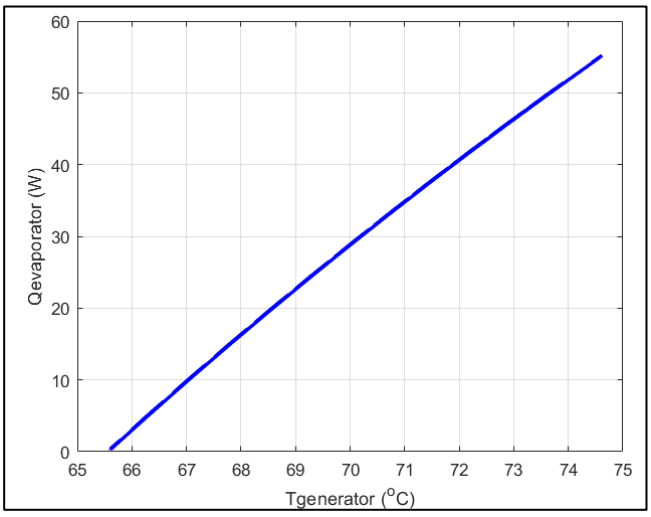

Fig. 19 The variation of Q_E with the generator temperature in March.

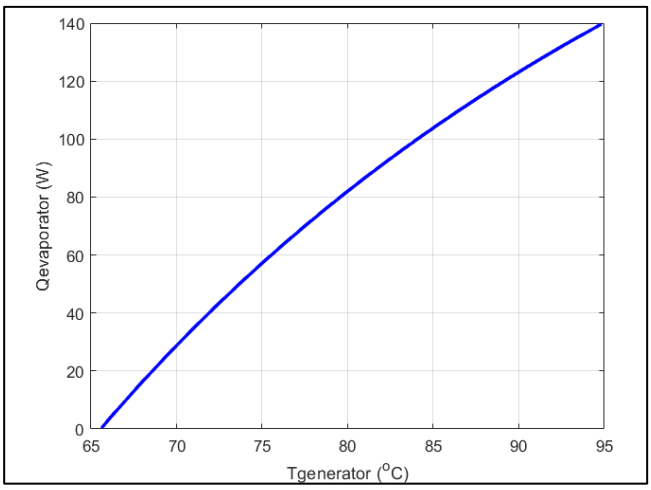

Fig. 20 The variation of Q_E with the generator temperature in July.

3.2.3. Coefficient of performance (COP)

Figure 21 shows that COP increases with increasing generator temperature in March. This is due to the increased amount of refrigerant separated in the generator, which enhances evaporation in the evaporator and increases cooling capacity. It is also noted that the rate of increase in COP begins to decrease at higher temperatures, indicating that the system is approaching its thermal performance limits in this month.

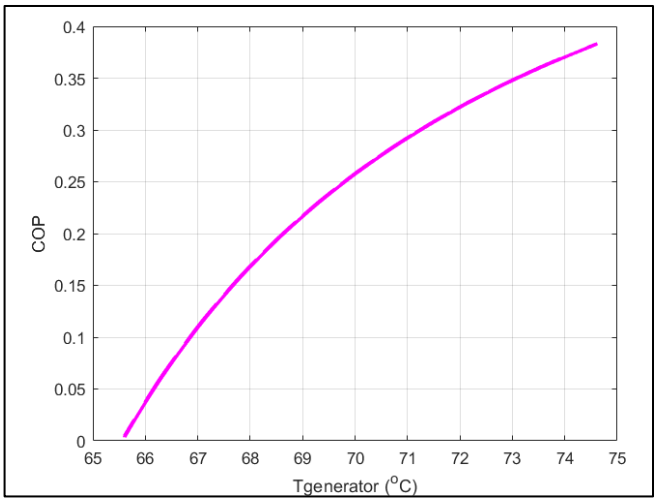

Fig. 21 The variation of COP with T_g the in March.

Figure 22 shows that COP is increasing as the generator temperature rises within the studied range for July (65.6-95 °C). This trend supports the dynamic concept of absorption cooling systems, as a rise in the generator (source) temperature is accompanied by an improved separation efficiency between the absorption medium (LiBr) and the coolant (water), which positively influences system performance.

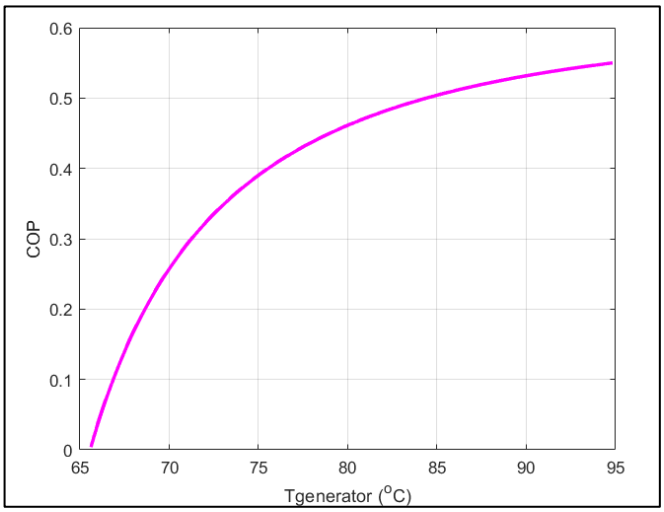

Fig. 22 The variation of COP with the generator temperature in July.

3.2.4. Validation of coefficient of performance (COP)

Figure 23 compares the simulation results of the coefficient of performance for an absorption refrigeration system using MATLAB with the theoretical study of COP from Kaynakli et al. [20]. The simulation parameters were: T_E = 2°C, T_C = T_A = 30, and ϵ_{HE} = 0. The figure shows good agreement between the simulation and theoretical results, especially when the generator temperature exceeds 70°C, where the values begin to converge slightly. It is also observed that the coefficient of performance increases with higher generator temperatures for both curves, reaching a nearly constant value of 0.7 between 80 and 85°C. This suggests that the system's thermal performance reaches a saturation point at these temperatures.

Conversely, a discrepancy appears at lower generator temperatures, notably at 62°C, where the simulation results are lower than those from Kaynakli et al. study. This difference likely stems from the mathematical solution method or

variations in assumptions. Overall, the mathematical model used in this study is considered accurate and reliable. The close alignment of the simulation results with published data strengthens the credibility of the model used to evaluate the performance of a lithium bromide-water absorption refrigeration system.

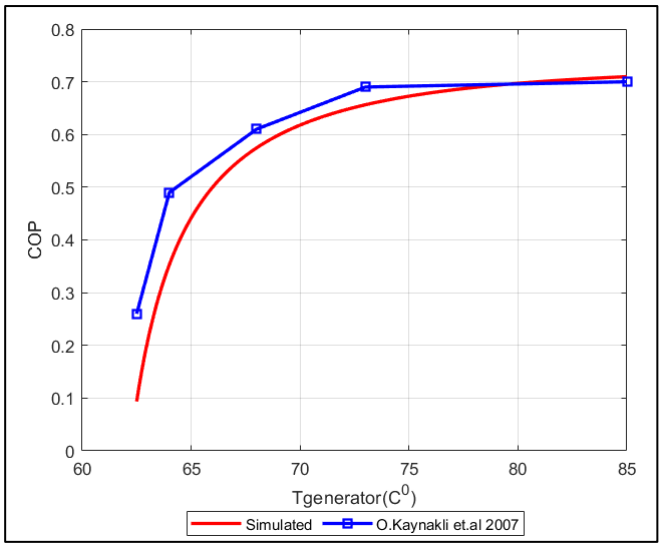

Fig. 23 Simulated and theoretical values of the coefficient of performance for Kaynakli et al. 2007 [20].

4. Conclusions

From the results, the following conclusions can be drawn:

1. This system relies on a renewable energy source, thereby contributing to reduced fossil fuel consumption. It is also environmentally friendly and efficient because it uses refrigerants that are non-harmful to the ozone layer.
2. This system generates clean energy that does not release harmful gases into the atmosphere, thereby not contributing to or exacerbating global warming.
3. The study demonstrated the feasibility of operating an absorption refrigeration system using the thermal energy stored in the lower layer of the solar pond, while maintaining good thermal stability in this layer throughout the day, especially in areas with high solar radiation.
4. The salt gradient within the solar pond effectively achieved thermal insulation between the layers, which helped reduce heat loss from the hot lower layers to the surface.
5. The impact of geographical location on the system's overall performance was significant, as the system's efficiency is heavily influenced by climatic conditions, particularly air temperature and solar radiation.
6. The maximum temperatures of the solar pond are reached during the summer months, peaking at 125°C in July. The lowest temperatures in the lower layer occur in December and January, at approximately 60°C.
7. The upper layer shows the lowest temperatures, while the non-convective zone (NCZ) has a temperature pattern similar to the lower layer but with moderate temperatures. The peak temperature reaches about 70°C in July, and the lowest temperatures are around 30°C in December and January.
8. July records the highest efficiency, exceeding 0.95, representing the optimal performance of the solar pond. The lowest efficiency value is recorded in March, where the efficiency declines by approximately 0.56.
9. Conclude that there is a direct relationship between generator temperature and the power output, with the Q_G value increases as the temperature in the generator rises. The highest Q_G value reached approximately 255 watts at a generator temperature of 95°C at the end of July, while the lowest value of 145 watts was recorded at about 74.6°C in March.
10. Conclude that July was the month with the best thermal performance, with Q_E reaching its peak value of over 135 watts at the end of July. However, Q_E fell below 60 watts in March.
11. The results show that achieving the highest possible system performance requires maintaining a high generator temperature. The highest Coefficient of Performance (COP) value was 0.56 at a generator temperature of 95°C in July, while the lowest Coefficient of Performance (COP) value was 0.38 at a generator temperature of approximately 74.7°C in March.

Nomenclature

Symbol	Description	Unit
A_{sp}	Area of the pond	m^2
C_p	Specific heat capacity of Salt water	J/kg ℃
θ_r	refraction angle at solar pond's surface	deg
h	convection heat transfer coefficient	W/m^2℃
h_{LCZ}	heat transfer coefficient in the LCZ	W/m^2℃
H_{Avg}	monthly solar radiation rate	W/m^2
H_O	total solar radiation	W/m^2
H_X	incoming radiation flux at depth x	W/m^2
J	diffusion flux	$kg/m^2\,s$
k	thermal conductivity of NaCl brine	W/m ℃
k_c	thermal conductivity of the tube	W/m ℃
LMTD	Log mean temperature difference	-
L_e	Lewis number	-
L_v	Latent heat of evaporation of water	kJ/kg
$\dot{m}$	Mass flow rate	kg/s
P_a	Partial pressure of vapor	mmHg
P_1	Vapor pressure at T_1	kPa
P_s	saturation vapor pressure	kPa
q_c	Heat transfer by convection	W/m^2
q_e	Heat transfer by evaporation	W/m^2
q_g	Heat loss to the ground	W/m^2
q_{loss}	Heat loss to the environment	W/m^2
q_r	Heat transfer by radiation	W/m^2
q_{cond}	Heat transfer by conduction	W/m^2
Q	Heat extraction rate	W/m^2
$\dot{Q}$	Total heat	kW
t	time	s
T	Temperature	℃
T_a	Ambient temperature	℃
T_{Sky}	Sky temperature	℃
U	Overall heat transfer coefficient	W/m^2 ℃
$R_{overall}$	Overall thermal resistance	m^2℃$/W$
V	Wind speed	m/s
x	depth	m
X_{UCZ}	Thickness of the UCZ	m
X_{NCZ}	Thickness of the NCZ	m
X_{LCZ}	Thickness of the LCZ	m
X_{ss}	strong solution concentration	-
X_{ws}	weak solution concentration	-

Subscripts

Symbol	Description
A	Absorber
C	Condenser
E	Evaporator
f	Fouling factors
G	Generator
i	inlet
o	outlet
ref	refrigerant

References

[1] M. Hawlader and B. Brinkworth, "An analysis of the non-convecting solar pond," Solar Energy, vol. 27, no. 3, pp. 195-204, 1981. https://doi.org/10.1016/0038-092X(81)90121-3

[2] A. R. Prasad, "Efficiency and thermal analysis of a salinity gradient solar pond," International Journal of a Scientific Research in Science, Engineering and Technology, vol. 2, no. 4, pp. 865-871, 2016.

[3] A. A. Monjezi and A. Campbell, "A comprehensive transient model for the prediction of the temperature distribution in a solar pond under Mediterranean conditions," Solar energy, vol. 135, pp. 297-307, 2016. https://doi.org/10.1016/j.solener.2016.06.011

[4] A. H. Sayer, An experimental and theoretical investigation of novel configurations of solar ponds for use in Iraq. University of Surrey (United Kingdom), 2017.

[5] A. Mohamed, A. Hegazi, G. Sultan, and E. M. El-Said, "Enhancement of a solar still performance by inclusion the basalt stones as a porous sensible absorber: experimental study and thermo-economic analysis," Solar Energy Materials and Solar Cells, vol. 200, p. 109958, 2019. https://doi.org/10.1016/j.solmat.2019.109958

[6] M. Li, C. Xu, R. H. E. Hassanien, Y. Xu, and B. Zhuang, "Experimental investigation on the performance of a solar powered lithium bromide–water absorption cooling system," International journal of refrigeration, vol. 71, pp. 46-59, 2016. https://doi.org/10.1016/j.ijrefrig.2016.07.023

[7] V. Yadav, N. Yadav, R. Bordia, R. Soni, and R. Khandey, "Design and Fabrication of Solar Powered Vapour Absorption Refrigeration System," in E3S Web of Conferences, 2020, vol. 170: EDP Sciences, p. 02011, https://doi.org/10.1051/e3sconf/202017002011

[8] A. Saleh, "Modeling and performance analysis of a solar pond integrated with an absorption cooling system," Energies, vol. 15, no. 22, p. 8327, 2022. https://doi.org/10.3390/en15228327

[9] T. W. Channel. "Monthly weather forecast for Basra Governorate," weather.com.

[10] V. V. N. Kishore and V. Joshi, "A practical collector efficiency equation for nonconvecting solar ponds," Solar Energy, vol. 33, no. 5, pp. 391-395, 1984. https://doi.org/10.1016/0038-092X(84)90190-7

[11] H. Kurt, F. Halici, and A. K. Binark, "Solar pond conception-experimental and theoretical studies," Energy conversion and management, vol. 41, no. 9, pp. 939-951, 2000. https://doi.org/10.1016/S0196-8904(99)00147-8

[12] S. Kanan, J. Dewsbury, and G. Lane-Serff, "A simple heat and mass transfer model for salt gradient solar ponds," in International Conference on Energy and Environmental Sciences, World Academy of Science, Engineering and Technology, pp. 27-33, 2014. https://doi.org/10.13140/2.1.1953.6328

[13] J. R. Hull, J. Nielsen, and P. Golding, "Salinity gradient solar ponds," 1988.

[14] J. Srinivasan, "Solar pond technology," Sadhana, vol. 18, pp. 39-55, 1993, https://doi.org/10.1007/BF02811386

[15] J. Leblanc, A. Akbarzadeh, J. Andrews, H. Lu, and P. Golding, "Heat extraction methods from salinity-gradient solar ponds and introduction of a novel system of heat extraction for improved efficiency," Solar Energy, vol. 85, no. 12, pp. 3103-3142, 2011. https://doi.org/10.1016/j.solener.2010.06.005

[16] M. R. Jaefarzadeh, "Heat extraction from a salinity-gradient solar pond using in pond heat exchanger," Applied Thermal Engineering, vol. 26, no. 16, pp. 1858-1865, 2006. https://doi.org/10.1016/j.applthermaleng.2006.01.022

[17] S. Ghatos, M. T. Janan, and A. Mehdari, "Thermodynamic model of a single stage H2O-LiBr absorption cooling," in E3S Web of Conferences, vol. 234, 2021. https://doi.org/10.1051/e3sconf/202123400091

[18] J. Huang, "A simple accurate formula for calculating saturation vapor pressure of water and ice," Journal of Applied Meteorology and Climatology, vol. 57, no. 6, pp. 1265-1272, 2018. https://doi.org/10.1175/JAMC-D-17-0334.1

[19] O. Ketfi, M. Merzouk, N. K. Merzouk, and S. El Metenani, "Performance of a single effect solar absorption cooling system (Libr-H_2O)," Energy procedia, vol. 74, pp. 130-138, 2015. https://doi.org/10.1016/j.egypro.2015.07.534

[20] O. Kaynakli and M. Kilic, "Theoretical study on the effect of operating conditions on performance of absorption refrigeration system," Energy conversion and management, vol. 48, no. 2, pp. 599-607, 2007. https://doi.org/10.1016/j.enconman.2006.06.005